

# **1 Differential response of a tree-killing bark beetle to forest structure 2 and composition across a gradient of climatic water deficit**

**3 Michael J. Koontz<sup>1,2,3\*</sup>, Andrew M. Latimer<sup>1,2</sup>, Leif A. Mortenson<sup>4</sup>, Christopher J. Fettig<sup>5</sup>, Malcolm P.  
4 North<sup>1,2,6</sup>**

**5** <sup>1</sup>Graduate Group in Ecology, University of California, Davis, CA, USA

**6** <sup>2</sup>Department of Plant Sciences, University of California, Davis, CA, USA

**7** <sup>3</sup>Earth Lab, University of Colorado-Boulder; Boulder, CO, USA

**8** <sup>4</sup>USDA Forest Service, Pacific Southwest Research Station, Placerville, CA, USA

**9** <sup>5</sup>USDA Forest Service, Pacific Southwest Research Station, Davis, CA, USA

**10** <sup>6</sup>USDA Forest Service, Pacific Southwest Research Station, Mammoth Lakes, CA, USA

**11** \*Correspondence: michael.koontz@colorado.edu

**12** *Keywords:* bark beetles, forest structure, drones, climatic water deficit, Sierra Nevada, California, disturbance,  
**13** structure from motion, *Dendroctonus brevicomis*, *Pinus ponderosa*, threshold dynamics

**14** *Abstract word count:* 336

**15** *Overall .docx word count:* 11096 *Main text word count:* 6967 (Intro: 1249; Methods: 3176  
**16** (679+647+1540+310); Results: 344 (41+102+201); Discussion: 2198)

**17** *Text boxes word count:* 0

**18** Date report generated: December 03, 2019

## **19 Abstract**

**20** The Californian hot drought of 2012 to 2015 created favorable conditions for unprecedented ponderosa pine  
**21** (*Pinus ponderosa*) mortality in the Sierra Nevada mountain range, largely attributable to the western pine  
**22** beetle (WPB; *Dendroctonus brevicomis*). Climate conditions and forest density may interact to affect tree  
**23** mortality, but density is a coarse gauge of forest structure that can affect WPB behavior in a number of  
**24** ways. Measuring broad-scale climate conditions simultaneously with local forest composition and structure–  
**25** the spatial distribution and size of trees– will refine our understanding of how these variables interact, but is  
**26** generally expensive and/or labor-intensive. We use drone surveys over a network of 160 field plots along a  
**27** 350km and 1000m elevation gradient in western slope Sierra Nevada ponderosa pine/mixed-conifer forests and  
**28** Structure from Motion processing to segment and classify more than 450,000 trees over 9km<sup>2</sup> of forest with  
**29** WPB-induced tree mortality. We modeled the probability of ponderosa pine mortality as a function of forest

30 structure and composition variables and their interaction with site-level climatic water deficit, accounting for  
31 spatial covariance using exact Gaussian processes. A greater local proportion of host trees strongly increased  
32 the probability of host mortality, with a greater host density amplifying this effect. Further, we found a  
33 strong interaction between host size and climatic water deficit such that larger trees increased the probability  
34 of host mortality at hot/dry sites, but smaller trees tended to drive mortality in cool/wet sites.  
35 Our results demonstrate a variable response of the WPB to local forest structure and composition across an  
36 environmental gradient, which may help reconcile differences between observed ecosystem-wide tree mortality  
37 patterns during the hot drought and predictions from models based on coarser-scale forest structure data.  
38 Climate change adaptation strategies should consider that future disturbance outcomes may depend on  
39 interactions between local forest structure and broad-scale environmental gradients, with the potential for  
40 cross-scale interactions to challenge our current understanding of forest insect dynamics.

## 41 Introduction

42 Bark beetles dealt the final blow to many of the nearly 150 million trees killed in the California hot drought of  
43 2012 to 2015 and its aftermath (USDAFS 2019). A harbinger of climate change effects to come, record high  
44 temperatures exacerbated the drought (Griffin and Anchukaitis 2014), which increased water stress on trees  
45 (Asner et al. 2016), making them more susceptible to colonization by bark beetles (Fettig 2012, Kolb et al.  
46 2016). Further, a century of fire suppression policy has enabled forests to grow into dense stands, which can  
47 also make them more vulnerable to bark beetles (Fettig 2012). This combination of environmental conditions  
48 and forest structural characteristics led to tree mortality events of unprecedented size in the driest, densest  
49 forests across the state (Young et al. 2017). The mechanisms underlying the link between tree susceptibility  
50 to colonization by insects and hot, dry conditions are often directly attributed to tree physiology (Bentz et al.  
51 2010), while the link to forest density is multifaceted (Fettig 2012). Because forest density is a coarse metric  
52 of the forest features to which bark beetles respond (Raffa et al. 2008), our understanding of the connection  
53 between forest density and insect disturbance severity could be enhanced with more finely-resolved measures  
54 of forest structure as well as explicit consideration of species composition (Stephenson et al. 2019, Fettig et al.  
55 2019). Finally, the challenge of simultaneously measuring the effects of both local-scale forest features (such  
56 as structure and composition) and broad-scale environmental conditions on forest insect disturbance leaves  
57 their interaction effect relatively underexplored (Seidl et al. 2016, Stephenson et al. 2019, Fettig et al. 2019).  
58 The ponderosa pine/mixed-conifer forests in California's Sierra Nevada region are characterized by regular  
59 bark beetle disturbances, primarily by the influence of western pine beetle (*Dendroctonus brevicomis*; WPB)  
60 on its host ponderosa pine (*Pinus ponderosa*) (Fettig 2016). The WPB is a "primary" bark beetle—its

61 reproductive success is contingent upon host tree mortality, which itself requires enough beetles to “mass  
62 attack” the host tree and overwhelm its defenses (Raffa and Berryman 1983). This Allee effect creates a  
63 strong coupling between beetle selection behavior of host trees and host tree susceptibility to colonization  
64 (Raffa and Berryman 1983, Logan et al. 1998). A key defense mechanism of trees to bark beetle attack is to  
65 flood beetle bore holes with resin, which physically expels beetles and may interrupt beetle communication  
66 (Franceschi et al. 2005, Raffa et al. 2015). Under normal conditions, weakened trees with compromised  
67 defenses are the most susceptible to colonization and will be the main targets of primary bark beetles like  
68 the western pine beetle (Bentz et al. 2010, Raffa et al. 2015). Under severe water stress, many trees no  
69 longer have the resources available to mount a defense (Kolb et al. 2016) and thus prolonged drought can  
70 often trigger increased bark beetle-induced tree mortality as average tree vigor declines (Bentz et al. 2010).  
71 As local population density of beetles increases due to successful reproduction within spatially-aggregated  
72 weakened trees, as might occur during drought, mass attacks grow in size and become capable of overwhelming  
73 formidable tree defenses such that even healthy trees may be susceptible to colonization and mortality (Bentz  
74 et al. 2010, Raffa et al. 2015). Thus, water stress can be a key determinant of whether individual trees are  
75 susceptible to bark beetles under many conditions, and this environmental condition may interact with beetle  
76 population dynamics to drive tree susceptibility under extreme conditions (Bentz et al. 2010, Stephenson et  
77 al. 2019).

78 Western pine beetle activity is strongly influenced by forest structure– the spatial distribution and size of  
79 trees– and tree species composition. Taking forest structure alone, high-density forests are more prone to  
80 bark beetle-induced tree mortality (Fettig 2012) which may arise as greater competition for water resources  
81 amongst crowded trees and thus average tree resistance is lower (Hayes et al. 2009), or because smaller gaps  
82 between trees protect pheromone plumes from dissipation by the wind and thus enhance intraspecific beetle  
83 communication (Thistle et al. 2004). Tree size is another aspect of forest structure that affects bark beetle  
84 host selection behavior with smaller trees tending to have lower capacity for resisting attack, and larger  
85 trees being a more desirable target on account of their thicker phloem providing greater nutritional content  
86 (Chubaty et al. 2009, Graf et al. 2012). Taking forest composition alone, WPB activity in the Sierra Nevada  
87 range of California is necessarily tied to the regional distribution of its exclusive host, ponderosa pine (Fettig  
88 2016). Colonization by primary bark beetles can also depend on the relative frequencies of tree species in a  
89 more local area, akin to reduced oligophagous insect herbivory in forests comprising taxonomically distinct  
90 tree species compared to monocultures (Jactel and Brockerhoff 2007). The interaction between forest structure  
91 and composition also drives WPB activity. For instance, high density forests with high host availability may  
92 experience greater beetle-induced tree mortality because dispersal distances between potential host trees are

93 shorter and facilitate successful colonization (Miller and Keen 1960, Berryman 1982, Fettig et al. 2007) or  
94 because high host availability reduces the chance of individual beetles wasting their limited resources flying  
95 to and landing on a non-host tree (Moeck et al. 1981, Evenden et al. 2014). Stand-scale measures of forest  
96 structure and composition thus paint a fundamentally limited picture of the mechanisms by which these  
97 forest characteristics affect bark beetle disturbance, but finer-grain information explicitly recognizing tree  
98 size, species, and local tree density should more appropriately capture the ecological processes underlying  
99 insect-induced tree mortality. Additionally, considering the effects of local forest structure and composition  
100 with the effects of environmental conditions may help refine our understanding of tree mortality patterns in  
101 widespread events such as during the recent California hot drought.

102 The vast spatial extent of tree mortality in the 2012 to 2015 California hot drought challenges our ability to  
103 simultaneously consider how broad-scale environmental conditions may interact with local forest structure  
104 and composition to affect the dynamic between bark beetle selection and colonization of host trees, and host  
105 tree susceptibility to attack (Anderegg et al. 2015, Stephenson et al. 2019). Measuring local forest structure  
106 generally requires expensive instrumentation (Kane et al. 2014, Asner et al. 2016) or labor-intensive field  
107 surveys (Larson and Churchill 2012, Stephenson et al. 2019, Fettig et al. 2019), which constrains survey  
108 extent and frequency. Small, unhumanned aerial systems (sUAS) enable relatively fast and cheap remote  
109 imaging over dozens of hectares of forest, which can be used to measure complex forest structure at the  
110 individual tree scale (Morris et al. 2017, Shiklomanov et al. 2019). Distributing such surveys across an  
111 environmental gradient can overcome the data acquisition challenge inherent in investigating phenomena  
112 with both a strong local- and a strong broad-scale component.

113 We used ultra-high resolution, sUAS-derived remote sensing data over a network of 32 sites in Sierra Nevada  
114 ponderosa pine/mixed-conifer forests spanning 1000m of elevation and 350km of latitude (see Fettig et al.  
115 (2019)) and covering a total of 9km<sup>2</sup> to ask how broad-scale environmental conditions interacted with local,  
116 complex forest structure to affect the probability of tree mortality during the cumulative tree mortality event  
117 of 2012 to 2018. We asked:

- 118 1. How does host tree density and average host tree size affect WPB-induced tree mortality?
- 119 2. How does the density of all tree species (hereafter “overall density”) and average tree size of all species  
120 (hereafter “overall size”) affect WPB-induced tree mortality?
- 121 3. How does environmentally-driven tree moisture stress affect WPB-induced tree mortality?
- 122 4. Do the effects of forest structure, forest composition, and environmental condition interact to influence  
123 WPB-induced tree mortality?

<sup>124</sup> **Methods**

<sup>125</sup> **Study system**

<sup>126</sup> We built our study coincident with 160 vegetation/forest insect monitoring plots at 32 sites established  
<sup>127</sup> between 2016 and 2017 by Fettig et al. (2019) (Figure 1). The study sites were chosen to reflect typical  
<sup>128</sup> west-side Sierra Nevada yellow pine/mixed-conifer forests and were dominated by ponderosa pine trees, *Pinus*  
<sup>129</sup> *ponderosa* (Fettig et al. 2019). These established plots were located in WPB-attacked, yellow pine/mixed-  
<sup>130</sup> conifer forests across the Eldorado, Stanislaus, Sierra and Sequoia National Forests and were stratified by  
<sup>131</sup> elevation (914-1219 m [3000-4000 ft], 1219-1524 m [4000-5000 ft], 1524-1829 m [5000-6000 ft] above sea level).  
<sup>132</sup> In the Sequoia National Forest, the southernmost National Forest in our study, plots were stratified with the  
<sup>133</sup> lowest elevation band between 1219 and 1524 m (4000-5000 ft) and extended to an upper elevation band of  
<sup>134</sup> 1829-2134 m (6000-7000 ft) to capture a more similar forest community composition as at the more northern  
<sup>135</sup> National Foxrests. The sites have variable forest structure and plot locations were selected in areas with  
<sup>136</sup> >35% ponderosa pine basal area and >10% ponderosa pine mortality. At each site, five 0.041 ha circular  
<sup>137</sup> plots were installed along transects with 80 to 200m between plots. In the field, Fettig et al. (2019) mapped  
<sup>138</sup> all stem locations relative to the center of each plot using azimuth/distance measurements. Tree identity to  
<sup>139</sup> species, tree height, and diameter at breast height (DBH) were recorded if DBH was greater than 6.35cm.  
<sup>140</sup> Year of mortality was estimated based on needle color and retention, if it wasn't directly observed during  
<sup>141</sup> site visits. A small section of bark (approximately 625 cm<sup>2</sup>) on both north and south aspects was removed  
<sup>142</sup> from dead trees to determine if bark beetle galleries were present. The shape, distribution, and orientation of  
<sup>143</sup> galleries are commonly used to distinguish among bark beetle species (Fettig 2016). In some cases, deceased  
<sup>144</sup> bark beetles were present beneath the bark to supplement identifications based on gallery formation. During  
<sup>145</sup> the spring and early summer of 2018, all field plots were revisited to assess whether dead trees had fallen  
<sup>146</sup> (Fettig et al. 2019).

<sup>147</sup> In the typical life cycle of western pine beetles, female WPB initiate host colonization by tunneling through  
<sup>148</sup> the outer bark and into the phloem and outer xylem where they rupture resin canals. As a result, oleoresin  
<sup>149</sup> exudes and collects on the bark surface, as is commonly observed with other bark beetle species. During the  
<sup>150</sup> early stages of attack, females release an aggregation pheromone component which, in combination with host  
<sup>151</sup> monoterpenes released from pitch tubes, is attractive to conspecifics (Bedard et al. 1969). An antiaggregation  
<sup>152</sup> pheromone component is produced during latter stages of host colonization by several pathways, and is  
<sup>153</sup> thought to reduce intraspecific competition by altering adult behavior to minimize overcrowding of developing  
<sup>154</sup> brood within the host (Byers and Wood 1980). Volatiles from several nonhosts sympatric with ponderosa pine  
<sup>155</sup> have been demonstrated to inhibit attraction of WPB (Shepherd et al. 2007, Fettig and Hilszczański 2015).

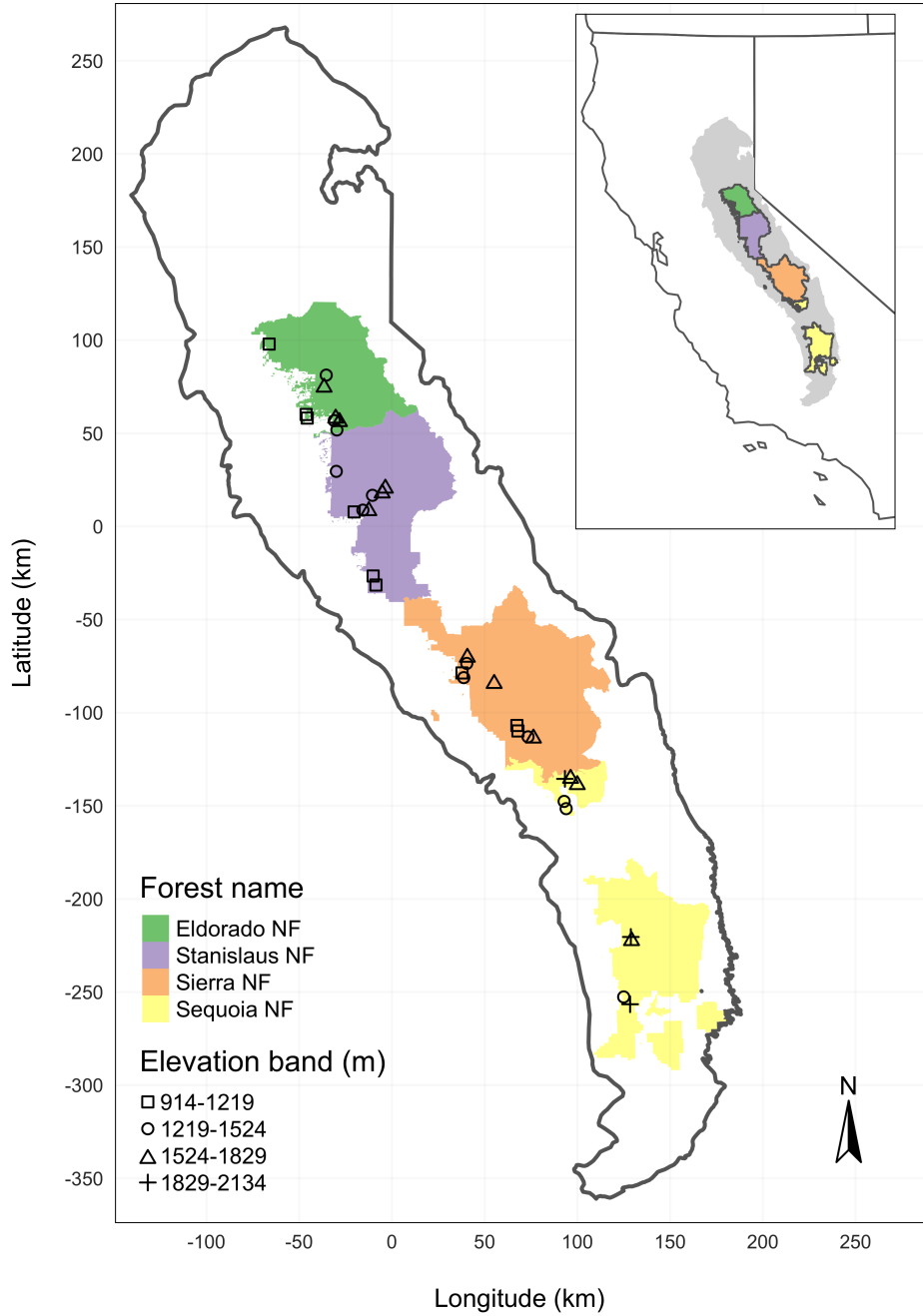


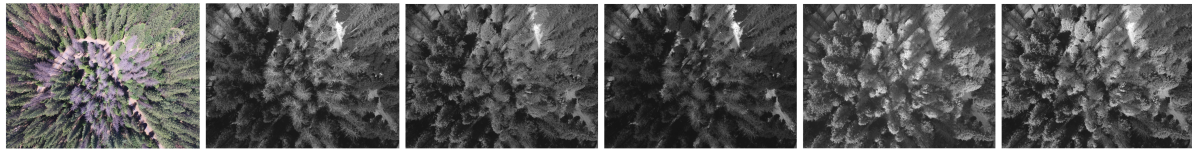
Figure 1: The network of field plots spanned a 350 km latitudinal gradient from the Eldorado National Forest in the north to the Sequoia National Forest in the south. Plots were stratified by three elevation bands in each forest, with the plots in the Sequoia National Forest (the southern-most National Forest) occupying elevation bands 305m above the three bands in the other National Forests in order to capture a similar community composition.

156 In California, the WPB can have 2-3 generations in a single year and can often out-compete its congener, the  
157 mountain pine beetle, *Dendroctonus ponderosa* (MPB), for the ponderosa pine host especially in larger trees  
158 (Miller and Keen 1960, Fettig 2016).

159 **Aerial data collection and processing**

160 Nadir-facing imagery was captured using a gimbal-stabilized DJI Zenmuse X3 broad-band red/green/blue  
161 (RGB) camera (DJI 2015a) and a fixed-mounted Micasense Rededge3 multispectral camera with five narrow  
162 bands (Micasense 2015) on a DJI Matrice 100 aircraft (DJI 2015b). Imagery was captured from both cameras  
163 along preprogrammed aerial transects over ~40 hectares surrounding each of the 36 sites (each of these  
164 containing five field plots) and was processed in a series of steps to yield local forest structure and composition  
165 data suitable for our statistical analysis. Following the call by Wyngaard et al. (2019), we establish “data  
166 product levels” to reflect the image processing pipeline from raw imagery (Level 0) to calibrated, fine-scale  
167 forest structure and composition information on regular grids (Level 4), with each new data level derived  
168 from levels below it. Here, we outline the steps in the processing and calibration pipeline visualized in Figure  
169 2, and include additional details in the Supplemental Methods.

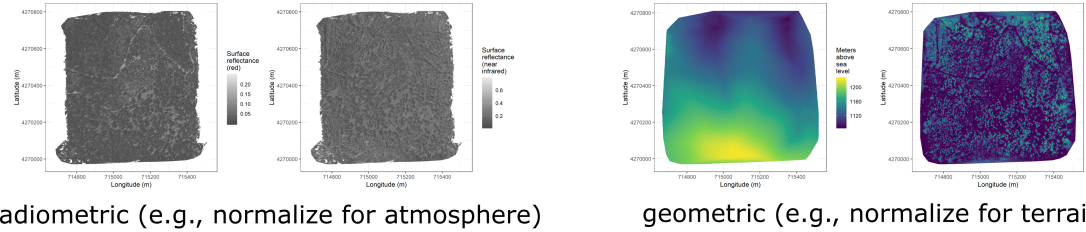
## Level 0: raw data from sensors



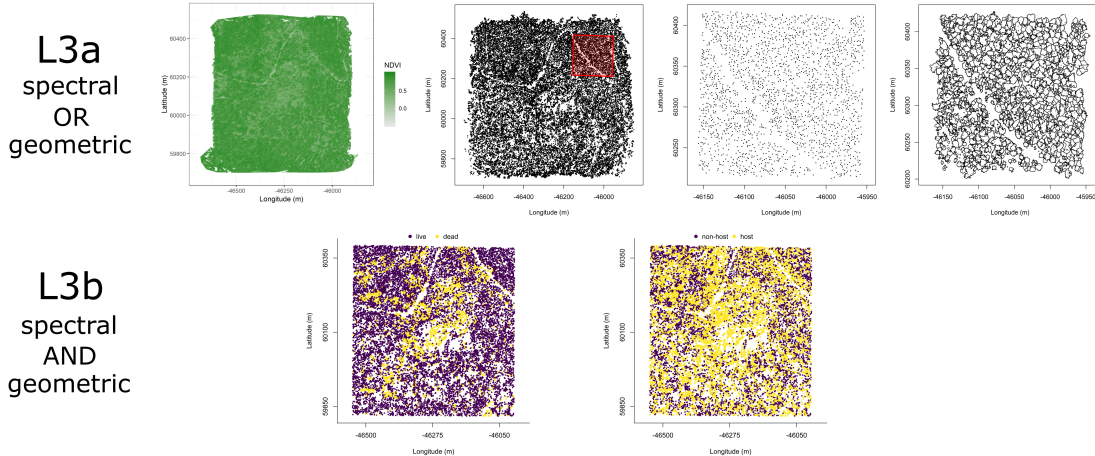
## Level 1: basic outputs from photogrammetric processing



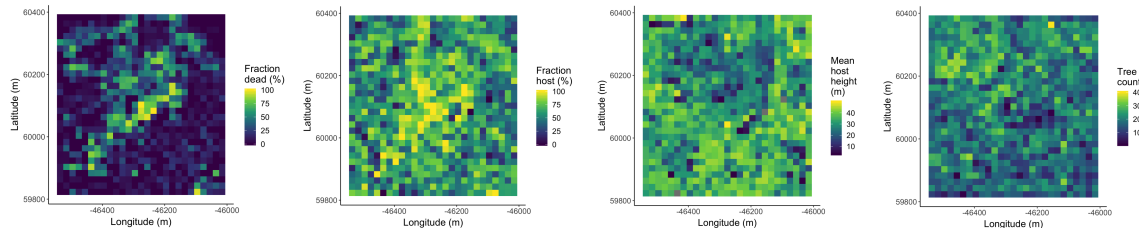
## Level 2: corrected outputs from photogrammetric processing



## Level 3: domain-specific information extraction



## Level 4: aggregations to regular grids



171 Figure 2. Schematic of the data processing workflow for a single site with each new data product level derived  
172 from data at lower levels.

173 Level 0 represents raw data from the sensors. From left to right: example broad-band RGB photo from  
174 DJI Zenmuse X3 camera, example blue photo from Rededge3 (centered on 475nm), example green photo  
175 from Rededge3 (centered on 560nm), example red photo from Rededge3 (centered on 668nm), example near  
176 infrared photo from Rededge3 (centered on 840nm), and example red edge photo from Rededge3 (centered on  
177 717nm).

178 Level 1 represents basic outputs from the photogrammetric workflow, in this case implemented with  
179 Pix4Dmapper. From left to right: a dense point cloud visualized in CloudCompare (<https://www.danielgm.net/cc/>), an orthophoto generated from the RGB camera, and a digital surface model representing the  
180 altitude above sea level (ground height + vegetation height) for every cell.

182 Level 2 represents outputs from photogrammetric processing that have been corrected radiometrically or  
183 geometrically. From left to right: a radiometrically-corrected surface reflectance map of the red narrow band  
184 from the Rededge3 camera, a radiometrically-corrected surface reflectance map of the near infrared narrow  
185 band from the Rededge3 camera, a rasterized version of the digital terrain model derived by a geometric  
186 correction of the dense point cloud, and a canopy height model derived by subtracting the terrain height  
187 from the digital surface model.

188 Level 3 represents domain-specific information extraction from Level 2 products and is divided into two  
189 sub-levels. Level 3a products are derived using only spectral or only geometric data. From left to right: a  
190 reflectance map of Normalized Difference Vegetation Index (NDVI; Rouse et al. (1973)) derived using the red  
191 and near infrared Level 2 reflectance products, a map of points representing detected trees from the canopy  
192 height model with a red polygon highlighting the area presented in more detail for the next two images, a  
193 close-up of points representing detected trees, and a close-up of polygons representing segmented tree crowns.

194 Level 3b products are derived using both spectral and geometric data. From left to right: a map of the point  
195 locations of detected trees that have been classified as alive or dead based on the pixel values within each  
196 segmented tree crown and a map of the point locations of detected trees classified to WPB host/non-host  
197 using the same spectral information. Note that our study relies on the generation of Level 3a products in  
198 order to combine them and create Level 3b products, but this need not be the case. For instance, deep  
199 learning/neural net methods may be able to use both the spectral and geometric information from Level 2  
200 simultaneously to locate and classify trees in a scene and directly generate Level 3b products without a need  
201 to first generate the Level 3a products shown in this schematic.

202 Level 4 represents aggregations of Level 3 products to regular grids which might better reflect the grain size  
203 of the data for which we have the best calibration and thus the most confidence or which might provide  
204 new information not possible at an individual-tree level (e.g., average distance between trees in a small  
205 neighborhood) From left to right: aggregation of live/dead classified trees as fraction of dead trees in a 20 x  
206 20-m cell and aggregation of host/non-host classified trees as fraction of hosts in a 20 x 20-m cell. In our  
207 case, the 20 x 20-m aggregation produces a grid cell with an area of 400m<sup>2</sup>, which most closely matches the  
208 404m<sup>2</sup> area of the ground-based vegetation plots whose data we used in an aggregated form to calibrate our  
209 derivation of Level 3 products.

## 210 **Level 0: Raw data from sensors**

211 Raw data comprised approximately 1900 images per camera lens (one broad-band RGB lens and five narrow-  
212 band multispectral lenses) for each of the 32 sites (Figure 2; Level 0). Prior to the aerial survey, two strips  
213 of bright orange drop cloth (~100 cm x 15 cm) were positioned as an “X” over the permanent monuments  
214 marking the center of the 5 field plots from Fettig et al. (2019) (see Supplemental Figures).

215 We preprogrammed north-south aerial transects using Map Pilot for DJI on iOS flight software (Drones-  
216 MadeEasy 2018) at an altitude of 120 m above ground level (with “ground” defined using a 1-arc-second  
217 digital elevation model (Farr et al. 2007)). The resulting ground sampling distance was approximately 5  
218 cm/px for the Zenmuse X3 RGB camera and approximately 8 cm/px for the Rededge3 multispectral camera.  
219 We used 91.6% image overlap (both forward and side) at the ground for the Zenmuse X3 RGB camera and  
220 83.9% overlap (forward and side) for the Rededge3 multispectral camera.

## 221 **Level 1: Basic outputs from photogrammetric processing**

222 We used structure from motion (SfM) photogrammetry implemented in Pix4Dmapper Cloud ([www.pix4d.com](http://www.pix4d.com))  
223 to generate dense point clouds (Figure 2; Level 1, left), orthophotos (Figure 2; Level 1, center), and digital  
224 surface models (Figure 2; Level 1, right) for each field site (Frey et al. 2018). For 29 sites, we processed the  
225 Rededge3 multispectral imagery alone to generate these products. For three sites, we processed the RGB and  
226 the multispectral imagery together to enhance the point density of the dense point cloud. All SfM projects  
227 resulted in a single processing “block,” indicating that all images in the project were optimized and processed  
228 together. The dense point cloud represents x, y, and z coordinates as well as the color of millions of points  
229 per site. The orthophoto represents a radiometrically uncalibrated, top-down view of the survey site that  
230 preserves the relative x/y positions of objects in the scene. The digital surface model is a rasterized version  
231 of the dense point cloud that shows the altitude above sea level for each pixel in the scene at the ground

232 sampling distance of the camera that generated the Level 0 data.

233 **Level 2: Corrected outputs from photogrammetric processing**

234 **Radiometric corrections**

235 A radiometrically-corrected reflectance map (Figure 2; Level 2, left two figures; i.e., a corrected version of the  
236 Level 1 orthophoto) was generated using the Pix4D software by incorporating incoming light conditions for  
237 each narrow band of the Rededge3 camera (captured simultaneously with the Rededge3 camera using an  
238 integrated downwelling light sensor) as well as a pre-flight image of a calibration panel of known reflectance  
239 (see Supplemental Methods for camera and calibration panel details).

240 **Geometric corrections**

241 We implemented a geometric correction to the Level 1 dense point cloud and digital surface model by  
242 normalizing these data for the terrain underneath the vegetation. We generated the digital terrain model  
243 representing the ground underneath the vegetation at 1 meter resolution (Figure 2; Level 2, third image)  
244 by classifying each survey area's dense point cloud into "ground" and "non-ground" points using a cloth  
245 simulation filter algorithm (Zhang et al. 2016) implemented in the `lidR` (Roussel et al. 2019) package and  
246 rasterizing the ground points using the `raster` package (Hijmans et al. 2019). We generated a canopy height  
247 model (Figure 2; Level 2, fourth image) by subtracting the digital terrain model from the digital surface  
248 model.

249 **Level 3: Domain-specific information extraction**

250 **Level 3a: Data derived from spectral OR geometric Level 2 product**

251 Using just the spectral information from the radiometrically-corrected reflectance maps, we calculated several  
252 vegetation indices including the normalized difference vegetation index (NDVI; Rouse et al. (1973); Figure  
253 2; Level 3a, first image), the normalized difference red edge (NDRE; Gitelson and Merzlyak (1994)), the  
254 red-green index (RGI; Coops et al. (2006)), the red edge chlorophyll index ( $CI_{red\ edge}$ ; Clevers and Gitelson  
255 (2013)), and the green chlorophyll index ( $CI_{green}$ ; Clevers and Gitelson (2013)).

Table 1: Algorithm name, number of parameter sets tested for each algorithm, and references.

Algorithm	Parameter sets tested	Reference(s)
li2012	131	Li et al. (2012); Jakubowski et al. (2013); Shin et al. (2018)

Algorithm	Parameter sets tested	Reference(s)
lmfx	30	Roussel (2019)
localMaxima	6	Roussel et al. (2019)
multichm	1	Eysn et al. (2015)
ptrees	3	Vega et al. (2014)
vwf	3	Plowright (2018)
watershed	3	Pau et al. (2010)

Using just the geometric information from the canopy height model or terrain-normalized dense point cloud, we generated maps of detected trees (Figure 2; Level 3a, second and third images) by testing a total of 7 automatic tree detection algorithms and a total of 177 parameter sets (Table 1). We used the field plot data to assess each tree detection algorithm/parameter set by converting the distance-from-center and azimuth measurements of the trees in the field plots to x-y positions relative to the field plot centers distinguishable in the Level 2 reflectance maps as the orange fabric X's that we laid out prior to each flight. In the reflectance maps, we located 0 out of 160 field plot centers while some plot centers were obscured due to dense interlocking tree crowns or because a plot center was located directly under a single tree crown. For each of the 0 field plots with identifiable plot centers– the “validation field plots”, we calculated 7 forest structure metrics using the ground data collected by Fettig et al. (2019): total number of trees, number of trees greater than 15 meters, mean height of trees, 25<sup>th</sup> percentile tree height, 75<sup>th</sup> percentile tree height, mean distance to nearest tree neighbor, and mean distance to second nearest neighbor. For each tree detection algorithm and parameter set described above, we calculated the same set of 7 structure metrics within the footprint of the validation field plots. We calculated the Pearson’s correlation and root mean square error (RMSE) between the ground data and the aerial data for each of the 7 structure metrics for each of the 177 automatic tree detection algorithms/parameter sets. For each algorithm and parameter set, we calculated its performance relative to other algorithms as whether its Pearson’s correlation was within 5% of the highest Pearson’s correlation as well as whether its RMSE was within 5% of the lowest RMSE. We summed the number of forest structure metrics for which it reached these 5% thresholds for each algorithm/parameter set. For automatically detecting trees across the whole study, we selected the algorithm/parameter set that performed well across the most number of forest metrics (see Results).

We delineated individual tree crowns (Figure 2; Level 3a, fourth image) with a marker controlled watershed segmentation algorithm (Meyer and Beucher 1990) implemented in the **ForestTools** package (Plowright

279 2018) using the detected treetops as markers. If the automatic segmentation algorithm failed to generate  
280 a crown segment for a detected tree (e.g., often snags with a very small crown footprint), a circular crown  
281 was generated with a radius of 0.5 meters. If the segmentation generated multiple polygons for a single  
282 detected tree, only the polygon containing the detected tree was retained. Because image overlap decreases  
283 near the edges of the overall flight path and reduces the quality of the SfM processing in those areas, we  
284 excluded segmented crowns within 35 m of the edge of the survey area. Given the narrower field of view of  
285 the Rededge3 multispectral camera versus the X3 RGB camera whose optical parameters were used to define  
286 the ~40 hectare survey area around each site, as well as the 35 m additional buffering, the survey area at  
287 each site was ~30 ha (see Supplemental Methods).

#### 288 **Level 3b: Data derived from spectral AND geometric information**

289 We overlaid the segmented crowns on the reflectance maps from 20 sites spanning the latitudinal and elevation  
290 gradient in the study. Using QGIS (<https://qgis.org/en/site/>), we hand classified 564 trees as live/dead  
291 (Figure 3) and as one of 5 dominant species in the study area (*Pinus ponderosa*, *Pinus lambertiana*, *Abies*  
292 *concolor*, *Calocedrus decurrens*, or *Quercus kelloggii*) using the mapped ground data as a guide. Each tree was  
293 further classified as “host” for ponderosa pine or “non-host” for all other species (Fettig 2016). We extracted  
294 all the pixel values within each segmented crown polygon from the five, Level 2 orthorectified reflectance  
295 maps (one per narrow band on the Rededge3 camera) as well as from the five, Level 3a vegetation index  
296 maps using the *velox* package (Hunziker 2017). For each crown polygon, we calculated the mean value of  
297 the extracted Level 2 and Level 3a pixels and used them as ten independent variables in a five-fold cross  
298 validated boosted logistic regression model to predict whether the hand classified trees were alive or dead.  
299 For just the living trees, we similarly used all 10 mean reflectance values per crown polygon to predict tree  
300 species using a five-fold cross validated regularized discriminant analysis. The boosted logistic regression and  
301 regularized discriminant analysis were implemented using the *caret* package in R (Kuhn 2008). Finally, we  
302 used these models to classify all tree crowns in the data set as alive or dead (Figure 2; Level 3b, first image)  
303 as well as the species of living trees (Figure 2; Level 3b, second image).

#### 304 **Level 4: Aggregations to regular grids**

305 We rasterized the forest structure and composition data at a spatial resolution similar to that of the field  
306 plots to better match the grain size at which we validated the automatic tree detection algorithms. In each  
307 raster cell, we calculated: number of dead trees, number of ponderosa pine trees, total number of trees, and  
308 mean height of ponderosa pine trees. The values of these variables in each grid cell and derivatives from  
309 them were used for visualization and modeling. Here, we show the fraction of dead trees per cell (Figure 2;

310 Level 4, first image), the fraction of host trees per cell (Figure 2; Level 4, second image), the mean height of  
311 ponderosa pine trees in each cell (Figure 2; Level 4, third image), and the total count of trees per cell (Figure  
312 2; Level 4, fourth image).

313 **Note on assumptions about dead trees**

314 For the purposes of this study, we assumed that all dead trees were ponderosa pine and thus hosts colonized  
315 by WPB. This is a reasonably good assumption for our study area; for example, Fettig et al. (2019) found  
316 that 73.4% of dead trees in their coincident field plots were ponderosa pine. Mortality was concentrated in  
317 the larger-diameter classes and attributed primarily to WPB (see Fettig et al. (2019), Figure 5). The species  
318 contributing to the next highest proportion of dead trees was incense cedar which represented 18.72% of the  
319 dead trees in the field plots. While the detected mortality is most likely to be ponderosa pine, it is critical to  
320 interpret our results with this known limitation in mind.

321 **Environmental data**

322 We used climatic water deficit (CWD) (Stephenson 1998) from the 1981-2010 mean value of the basin  
323 characterization model (Flint et al. 2013) as an integrated measure of temperature and moisture conditions  
324 for each of the 32 sites. Higher values of CWD correspond to hotter, drier conditions and lower values  
325 correspond to cooler, wetter conditions. CWD has been shown to correlate well with broad patterns of tree  
326 mortality in the Sierra Nevada (Young et al. 2017) as well as bark beetle-induced tree mortality (Millar et al.  
327 2012). We converted the CWD value for each site into a z-score representing that site's deviation from the  
328 mean CWD across the climatic range of Sierra Nevada ponderosa pine as determined from 179 herbarium  
329 records described in Baldwin et al. (2017). Thus, a CWD z-score of 1 would indicate that the CWD at that  
330 site is one standard deviation hotter/drier than the mean CWD across all geolocated herbarium records for  
331 ponderosa pine in the Sierra Nevada.

332 **Statistical model**

333 We used a generalized linear model with a zero-inflated binomial response and a logit link to predict the  
334 probability of ponderosa pine mortality within each 20 x 20-m cell using the total number of ponderosa  
335 pine trees in each cell as the number of trials, and the number of dead trees in each cell as the number of  
336 "successes". As covariates, we used the proportion of trees that are WPB hosts (i.e., ponderosa pine) in  
337 each cell, the mean height of ponderosa pine trees in each cell, the density of trees of all species (hereafter  
338 "overall density") in each cell, and the site-level climatic water deficit using Eq. 1. Note that the two-way  
339 interaction between the overall density and the proportion of trees that are hosts is equivalent to the number

340 of ponderosa pine trees in the cell. To measure and account for spatial autocorrelation underlying ponderosa  
 341 pine mortality, we subsampled the data at each site to a random selection of 200, 20 x 20-m cells representing  
 342 approximately 27.5% of the surveyed area. Additionally with these subsampled data, we included a separate  
 343 exact Gaussian process term per site of the interaction between the x- and y-position of each cell using the  
 344 `gp()` function in the `brms` package (Bürkner 2017). The Gaussian process estimates the spatial covariance in  
 345 the response variable (log-odds of ponderosa pine mortality) jointly with the effects of the other covariates.

$$y_{i,j} \sim \begin{cases} 0, & p \\ Binom(n_i, \pi_i), & 1 - p \end{cases}$$

$$\begin{aligned}
 logit(\pi_i) = & \beta_0 + \\
 & \beta_1 X_{cwd,j} + \beta_2 X_{propHost,i} + \beta_3 X_{PIPOheight,i} + \beta_4 X_{overallDensity,i} + \\
 & \beta_5 X_{cwd,j} X_{PIPOheight,i} + \beta_6 X_{cwd,j} X_{propHost,i} + \beta_7 X_{cwd,j} X_{overallDensity,i} + \\
 & \beta_8 X_{propHost,i} X_{PIPOheight,i} + \beta_9 X_{propHost,i} X_{overallDensity,i} + \\
 & \beta_{10} X_{cwd,j} X_{propHost,i} X_{PIPOheight,i} + \\
 & \mathcal{GP}_j(x_i, y_i)
 \end{aligned}$$

346 Where  $y_i$  is the number of dead trees in cell  $i$ ,  $n_i$  is the sum of the dead trees (assumed to be ponderosa pine)  
 347 and live ponderosa pine trees in cell  $i$ ,  $\pi_i$  is the probability of ponderosa pine tree mortality in cell  $i$ ,  $p$  is the  
 348 probability of there being zero dead trees in a cell arising as a result of an unmodeled process,  $X_{cwd,j}$  is the  
 349 z-score of climatic water deficit for site  $j$ ,  $X_{propHost,i}$  is the scaled proportion of trees that are ponderosa  
 350 pine in cell  $i$ ,  $X_{PIPOheight,i}$  is the scaled mean height of ponderosa pine trees in cell  $i$ ,  $X_{overallDensity,i}$  is  
 351 the scaled density of all trees in cell  $i$ ,  $x_i$  and  $y_i$  are the x- and y- coordinates of the centroid of the cell in  
 352 an EPSG3310 coordinate reference system, and  $\mathcal{GP}_j$  represents the exact Gaussian process describing the  
 353 spatial covariance between cells at site  $j$ .

354 We used 4 chains with 4000 iterations each (2000 warmup, 2000 samples), and confirmed chain convergence  
 355 by ensuring all `Rhat` values were less than 1.1 (Brooks and Gelman 1998) and that the bulk and tail effective  
 356 sample sizes (ESS) for each estimated parameter were greater than 100 times the number of chains (i.e.,  
 357 greater than 400 in our case). We used posterior predictive checks to visually confirm model performance by  
 358 overlaying the density curves of the predicted number of dead trees per cell over the observed number (Gabry  
 359 et al. 2019). For the posterior predictive checks, we used 50 random samples from the model fit to generate  
 360 50 density curves and ensured curves were centered on the observed distribution, paying special attention to

361 model performance at capturing counts of zero.

## 362 Software and data availability

363 All data are available via the Open Science Framework. Statistical analyses were performed using the `brms`  
364 packages. With the exception of the SfM software (Pix4Dmapper Cloud) and the GIS software QGIS, all  
365 data carpentry and analyses were performed using R (R Core Team 2018).

## 366 Results

### 367 Tree detection algorithm performance

368 We found that the experimental `lmfx` algorithm with parameter values of `dist2d = 1` and `ws = 2.5` (Roussel  
369 et al. 2019) performed the best across 7 measures of forest structure as measured by Pearson's correlation  
370 with ground data (Table 2).

Table 2: Correlation and differences between the best performing tree detection algorithm (`lmfx` with `dist2d = 1` and `ws = 2.5`) and the ground data. An asterisk next to the correlation or RMSE indicates that this value was within 5% of the value of the best-performing algorithm/parameter set. Ground mean represents the mean value of the forest metric across the `r nrow(identifiable_plot_centers)` field plots that were visible from the sUAS-derived imagery. The median error is calculated as the median of the differences between the air and ground values for the `r nrow(identifiable_plot_centers)` visible plots. Thus, a positive number indicates an overestimate by the sUAS workflow and a negative number indicates an underestimate.

Forest structure metric	Ground mean	Correlation with ground	RMSE	Median error
total tree count	19	0.67*	8.68*	2
count of trees > 15m	9.9	0.43	7.38	0
distance to 1st neighbor (m)	2.8	0.55*	1.16*	0.26
distance to 2nd neighbor (m)	4.3	0.61*	1.70*	0.12
height (m); 25th percentile	12	0.16	8.46	-1.2
height (m); mean	18	0.29	7.81*	-2.3
height (m); 75th percentile	25	0.35	10.33*	-4

### 371 Classification accuracy for live/dead and host/non-host

372 The accuracy of live/dead classification on a withheld test dataset was 97.3%. The accuracy of species  
373 classification on a withheld testing dataset was 66.7%. The accuracy of WPB host/non-WPB-host (i.e.,  
374 ponderosa pine versus other tree species) on a withheld testing dataset was 74.4%.

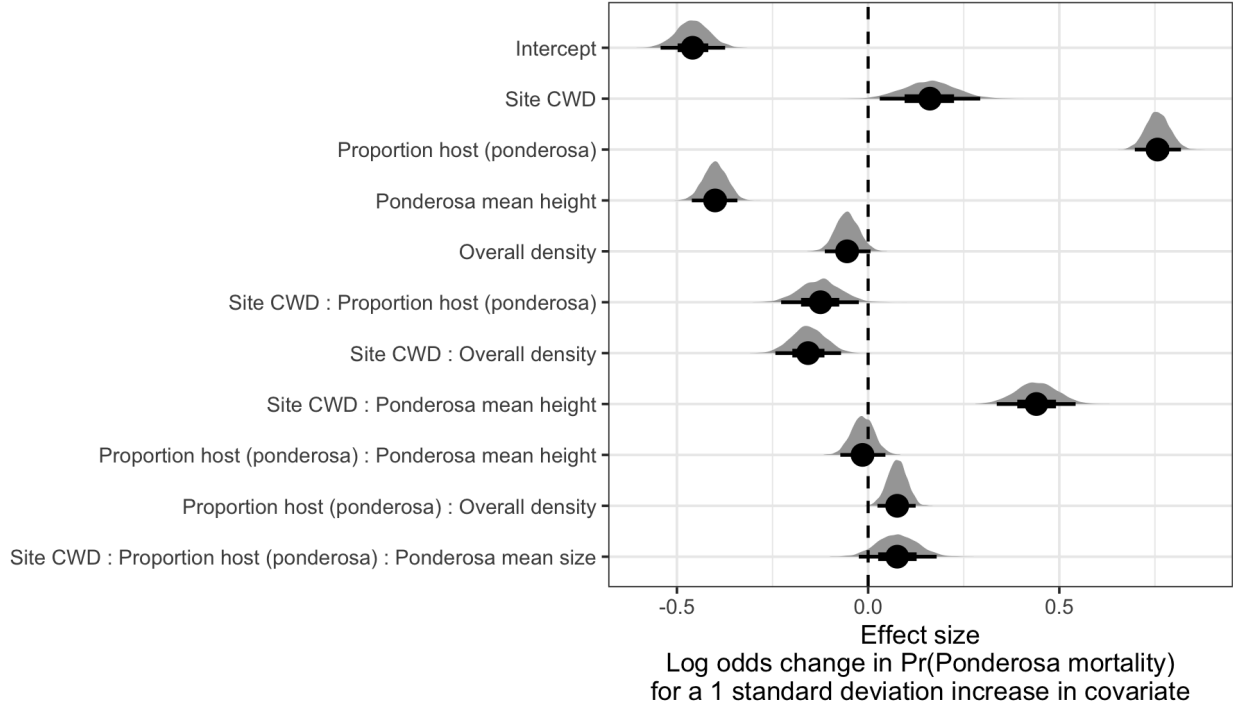


Figure 4: Posterior distributions of effect size from zero-inflated binomial model predicting the probability of ponderosa pine mortality in a 20 x 20-m cell given forest structure characteristics and site-level climatic water deficit. The gray density distribution for each model covariate represents the density of the posterior distribution, the point underneath each density curve represents the median of the estimate, the bold interval surrounding the point estimate represents the 66% credible interval, and the thin interval surrounding the point estimate represents the 95% credible interval.

### **375 Site summary based on best tree detection algorithm and classification**

**376** Across our study site, we detected, segmented, and classified 452,413 trees (see Supplemental Table for site  
**377** summaries). Of these trees, we classified 118,879 as dead (26.3% mortality). Estimated tree mortality at a  
**378** site ranged from 6.8% to 53.6%.

### **379 Effect of local structure and regional climate on tree mortality attributed to western pine **380 beetle****

**381** We detected a positive main effect of climatic water deficit on the probability of ponderosa pine mortality  
**382** within each 20 x 20-m cell (Figure 4). We found a positive main effect of proportion of host trees per cell,  
**383** with a greater proportion of host trees (i.e., ponderosa pine) in a cell increasing the probability of ponderosa  
**384** pine mortality. Conversely, we found a negative effect of overall tree density (i.e., including both ponderosa  
**385** pine and non-host species) such that greater tree density in a 20 x 20-m cell (for the same proportion of host  
**386** trees) would decrease the probability of ponderosa pine mortality. We found a positive two-way interaction

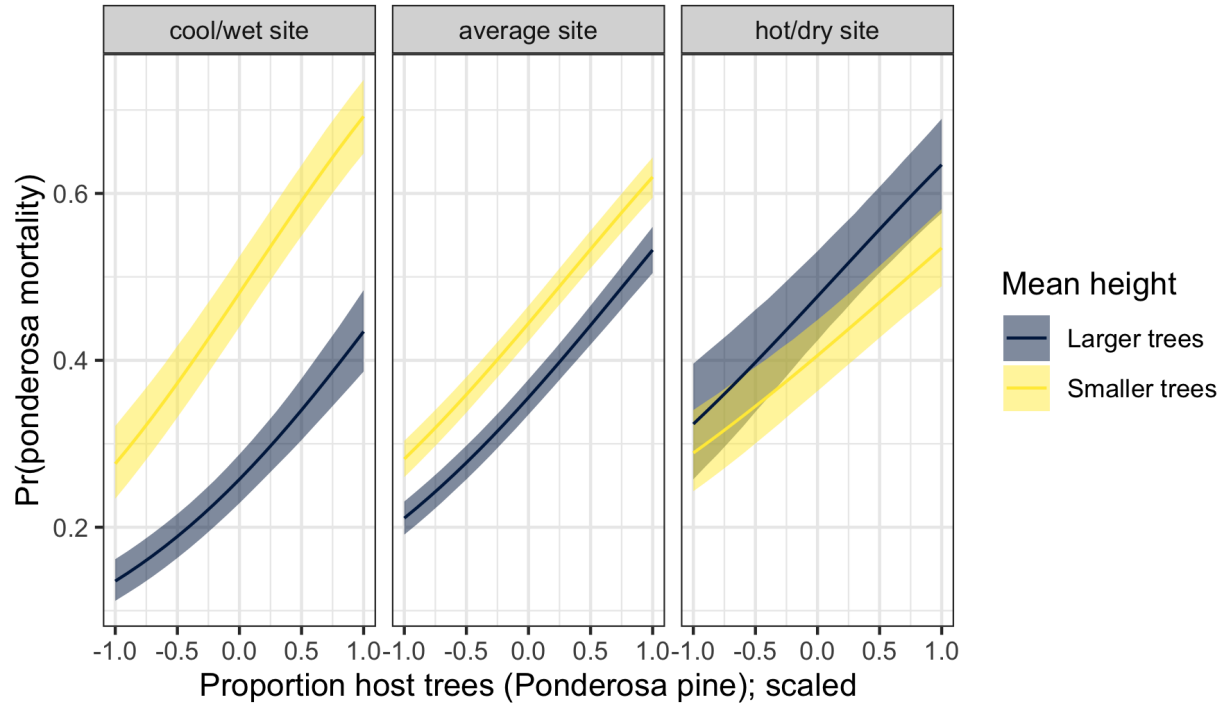


Figure 5: Line version of model results with 95% credible intervals showing primary influence of ponderosa pine structure on the probability of ponderosa pine mortality, and the interaction across climatic water deficit. The ‘larger trees’ line represents the mean height of ponderosa pine 0.7 standard deviations above the mean (approximately 12.1m), and the ‘smaller trees’ line represents the mean height of ponderosa pine 0.7 standard deviations below the mean (approximately 24.1m).

387 between the overall tree density per cell and the proportion of trees that were hosts, which is equivalent to a  
 388 positive effect of the density of host trees (Figure 4).  
 389 We found a negative effect of mean height of ponderosa pine on the probability of ponderosa mortality,  
 390 suggesting that the western pine beetle attacked smaller trees, on average. However, there was a positive  
 391 interaction between the climatic water deficit and ponderosa pine mean height, such that larger trees were  
 392 more likely to increase the probability of ponderosa mortality in hotter, drier sites (Figure 5).  
 393 We found weakly negative effects of the site-level CWD interactions with both the proportion of host trees  
 394 and overall tree density (Figure 4).

## 395 Discussion

396 This study represents a novel use of drones to further our understanding of the simultaneous effects of  
 397 local forest structure and composition with broad-scale environmental gradients on tree mortality attributed  
 398 to WPB. We found strong positive effects (effect sizes >0.4) of both the proportion of host trees and the  
 399 interaction between site climatic water deficit (CWD) and host tree mean size (height) on the probability of

400 ponderosa pine mortality. Conversely, we found a strong negative effect (effect size <-0.4) of mean height of  
401 ponderosa pine. Site-level CWD exerted a positive, but relatively weak, main effect on the probability of  
402 ponderosa mortality (effect size: 0.16; 95% CI: [0.03, 0.29]). To that end, we did not measure tree water  
403 stress at an individual tree level as in other recent work (Stephenson et al. 2019), and instead treated CWD  
404 as a general indicator of tree stress following results of coarser-scale studies (Asner et al. 2016, Young et al.  
405 2017), which may have contributed to our failure to detect a stronger CWD effect. Also, our entire study area  
406 experienced the same extreme hot drought between 2012 and 2015 and the variation of mortality explained  
407 by a main effect of climatic water deficit may be dampened when most trees are experiencing a high degree  
408 of water stress (Floyd et al. 2009, Fettig et al. 2019).

#### 409 **Positive effect of host density and a negative effect of overall density**

410 The strongest effect on the probability of ponderosa pine mortality was the positive effect of the proportion  
411 of trees in each 20 x 20-m cell that were ponderosa pine– the host of the WPB (effect size: 0.76; 95% CI:  
412 [0.70, 0.82]).

413 A number of mechanisms associated with the relative abundance of species in a local area might underlie  
414 this relationship. Frequency-dependent herbivory–whereby mixed-species forests experience less herbivory  
415 compared to monocultures– is common, especially for oligophagous insect species (Jactel and Brockerhoff  
416 2007). Furthermore, it has been demonstrated that nonhost volatiles reduce attraction of several species of  
417 bark beetles to their aggregation pheromones (Seybold et al. 2018), including WPB (Fettig et al. 2005). To  
418 that end, combinations of nonhost volatiles and an antiaggregation pheromone have been used successfully to  
419 reduce levels of tree mortality attributed to WPB (e.g., Fettig et al. (2012)). In general, Hayes et al. (2009)  
420 and Fettig et al. (2019) found that measures of host availability explained less variation in mortality than  
421 measures of overall tree density, but those conclusions were based on a response variable of “total number of  
422 dead host trees,” rather than the number of dead host trees conditional on the total number of host trees as  
423 in our study (i.e., a binomial response).

424 The negative relationship between overall tree density, a potential correlate of the local competitive envi-  
425 ronment, and the probability of ponderosa pine mortality is counter-intuitive but corroborates findings of  
426 coincident ground plots (Fettig et al. 2019) and other work during the same hot drought (Restaino et al.  
427 2019). The forest structure is itself a product of climate and, with increasing importance at finer spatial  
428 scales, topographic conditions (Fricker et al. 2019). Thus, the denser forest patches in our study may reflect  
429 locally favorable conditions for tree growth and survivorship which could enable increased resistance to insect  
430 attack (Restaino et al. 2019). The negative two-way interaction between site CWD and overall density that

431 amplifies the negative overall density effect in hotter, drier sites (effect size: -0.16; 95% CI: [-0.24, -0.07])  
432 supports this explanation if greater local tree density implies especially favorable growing conditions (and  
433 locally resistant trees) when denser patches are found in hot, dry sites.

434 We found a positive two-way interaction between overall tree density (host and non-host) within each cell  
435 and proportion of host trees, which is equivalent to a positive effect of host density (effect size: 0.08; 95% CI:  
436 [0.03, 0.12]), The relationship between host density and susceptibility to colonization by bark beetles has  
437 been so well-documented at the experimental plot level (e.g., Raffa and Berryman (1987), Oliver (1995)) that  
438 lowering stand densities through selective harvest of hosts is commonly recommended for reducing future  
439 levels of tree mortality attributed to bark beetles (Fettig and Hilszczański 2015), including WPB (Fettig  
440 2016). Greater host density shortens the flight distance required for WPB to disperse to new host, which  
441 likely facilitates bark beetle spread, but we calibrated our aerial tree detection to ~400 m<sup>2</sup> areas rather than  
442 to individual tree locations so don't have the data precision to address this hypothesis directly. Increased  
443 density of ponderosa pine, specifically, may disproportionately increase the competitive environment for these  
444 WPB host trees (and thus increase their susceptibility to WPB colonization) if intraspecific competition  
445 amongst ponderosa pine trees is stronger than interspecific competition as would be predicted with coexistence  
446 theory (Chesson 2000). Finally, greater host density likely increases the frequency that WPB land on their  
447 preferred host and avoid expending energy flying to non-hosts.

448 **Negative main effect of host tree mean size, but strong postive interaction with site CWD**

449 Counter to our expectations, we found an overall negative effect of host tree mean size on the probability of  
450 host mortality (effect size: -0.40; 95% CI: [-0.46, -0.34]). WPB exhibit a preference for trees 50.8 to 76.2 cm  
451 in diameter at breast height (Person 1928, 1931), and a positive relationship between host tree size and levels  
452 of tree mortality attributed to WPB was reported by Fettig et al. (2019) in the coincident field plots as well  
453 as in other recent studies (Restaino et al. 2019, Stephenson et al. 2019, Pile et al. 2019). Indeed, Fettig et al.  
454 (2019) reported no mortality in ponderosa pine trees < 10.0 cm dbh and found no relationship between tree  
455 size and tree mortality for incense cedar or white fir in the coincident field plots. These species represent  
456 22.3% of the total tree mortality observed in their study, yet in our study all dead trees were classified as  
457 ponderosa pine (see Methods) which could dampen positive effect of tree size on mortality. Larger trees  
458 are more nutritious and are therefore ideal targets if local bark beetle density is high enough to successfully  
459 initiate mass attack as can occur when many trees are under severe water stress (Bentz et al. 2010). In the  
460 recent hot drought, we expected that most trees would be under severe water stress, setting the stage for  
461 increasing beetle density, successful mass attacks, and targeting of larger trees. A possible explanation for

462 our finding counter to this expectation is that our observations represent the cumulative mortality of trees  
463 during a multi-year drought event and its aftermath. Lower host tree mean size led to a greater probability  
464 of host mortality earlier in this drought (Pile et al. 2019, Stovall et al. 2019) and that signal might have  
465 persisted even as mortality continued to accumulate driven by other factors. Finally, tree growth rates may  
466 be a better predictor of susceptibility to WPB colonization than tree size per se, with slower-growing trees  
467 being most vulnerable (Miller and Keen 1960). While slow-growing trees are often also the largest trees, this  
468 may not be the case for our study sites especially given the legacy of fire exclusion in the Sierra Nevada and  
469 its effect of perturbing forest structure far outside its natural range of variation (Safford and Stevens 2017).

470 We did observe a strong host tree size effect in its interaction with site CWD (effect size: 0.44; 95% CI:  
471 [0.34, 0.54]). In hot, dry sites, larger average host size increased the probability of host mortality while  
472 smaller host sizes increased the probability of host mortality in cooler, wetter sites. Notably, a similar pattern  
473 was shown by Stovall et al. (2019) with a strong positive tree height/mortality relationship in areas with  
474 the greatest vapor pressure deficit and no tree height/mortality relationship in areas with the lowest vapor  
475 pressure deficit. Stovall et al. (2019) did not observe that this environmental dependence extended to a  
476 negative tree height/mortality relationship (as we did) even at the lowest extremes of their VPD gradient,  
477 perhaps because their entire study took place in the southern Sierra Nevada which represents a hotter, drier  
478 portion of the more spatially extensive results we present here. Our work suggests that the WPB was cueing  
479 into different aspects of forest structure across an environmental gradient in a spatial context in a parallel  
480 manner to the temporal context noted by Stovall et al. (2019) and Pile et al. (2019), who observed that  
481 mortality was increasingly driven by larger trees as the hot drought proceeded and became more severe.

482 All of our sites were considered in an “epidemic” population phase for WPB (>5 trees killed per hectare;  
483 see supplemental information; Miller and Keen (1960), Hayes et al. (2009)), but our results challenge the  
484 notion that outbreak behavior by the WPB and subsequent tree mortality is always driven by greater tree  
485 size. Despite a strong tree size/mortality relationship in coincident ground plots across our study area (Fettig  
486 et al. 2019), our results from surveying the broader context surrounding those ground plots reveals different  
487 effects of host tree size depending on CWD. Thus, it is possible that massive mortality in hotter/drier Sierra  
488 Nevada forests (lower latitudes and elevations) (Asner et al. 2016, Young et al. 2017) during the 2012-2015  
489 hot drought arose as a synergistic alignment of environmental conditions and local forest structure allowed  
490 WPB to successfully colonize large trees, rapidly increase in population size, and expand. Conversely, our  
491 results may suggest that the unexpectedly low mortality in cooler/wetter Sierra Nevada forests compared  
492 to model predictions based on coarser-scale forest structure data (Young et al. 2017) could be explained  
493 by a different WPB response to local forest structure due to a lack of an alignment with favorable climate

494 conditions.

## 495 **Limitations and future directions**

496 We have demonstrated that drones can be effective means of collecting forest data at multiple, vastly different  
497 spatial scales to investigate a single, multi-scale phenomenon— from meters in between trees, to hundreds  
498 of meters of elevation, to hundreds of thousands of meters of latitude. Some limitations remain but can be  
499 overcome with further refinements in the use of this tool for forest ecology. Most of these limitations arise  
500 from tree detection and classification uncertainty, and thus it was imperative to work with field data for  
501 calibration and uncertainty reporting.

502 The greatest limitation in our study arising from classification uncertainty is in the assumption that all dead  
503 trees were ponderosa pine. We estimate from coincident field plots that this is true approximately 73.4%  
504 of the time. While spectral information of foliage could help classify living trees to species, standing dead  
505 trees did not reflect differently for different species. Because tree mortality response to forest insects is  
506 species-specific, even with sympatric tree species during the same hot drought (Stephenson et al. 2019), we  
507 cannot entirely rule out that some of the mortality responses to complex forest structure that we observed  
508 arose from these species-specific responses. The overall community composition across our study area was not  
509 very different (Fettig et al. 2019), so we remain confident that the patterns we observed were driven primarily  
510 by the dynamic between the western pine beetle and ponderosa pine. This challenge of classifying standing  
511 dead trees to species implies that a conifer forest system with less bark beetle and tree host diversity, such as  
512 mountain pine beetle-induced mortality in monocultures of lodgepole pine, should be particularly amenable  
513 to the methods presented here even with minimal further refinement because a dead tree will almost certainly  
514 belong to a single species and have succumbed due to bark beetle colonization.

515 Some uncertainty surrounded our ability to detect trees using the geometry of the dense point clouds derived  
516 with SfM. The horizontal accuracy of the tree detection was better than the vertical accuracy, which may  
517 result from a more significant error contribution by the field-based calculations of tree height compared to  
518 tree position relative to plot center (Table 2). Both the horizontal and vertical accuracy would likely improve  
519 with better SfM point clouds, which can be enhanced with greater overlap between images (Frey et al. 2018)  
520 or with oblique (i.e., off-nadir) imagery (James and Robson 2014). Frey et al. (2018) found that 95% overlap  
521 was preferable for generating dense point clouds in forested areas, and James and Robson (2014) reduced  
522 dense point cloud errors using imagery taken at 30 degrees off-nadir. We only achieved 91.6% overlap with  
523 the X3 RGB camera and 83.9% overlap with the multispectral camera, and all imagery was nadir-facing.  
524 While our live/dead classification was fairly accurate (97.3% on a withheld dataset), our species classifier

would likely benefit from better crown segmentation because the pixel-level reflectance values within each crown are averaged to characterize the “spectral signature” of each tree. With better delineation of each tree crown, the mean value of pixels within each tree crown will likely be more representative of that tree’s spectral signature. Better crown segmentation would most readily be achieved through greater overlap in imagery. Finally, we anticipate that computer vision and deep learning will prove helpful in overcoming some of these detection and classification challenges (Gray et al. 2019).

## Conclusions

Climate change adaptation strategies emphasize management action that considers whole-ecosystem responses to inevitable change (Millar et al. 2007), which requires a macroecological understanding of how phenomena at multiple scales can interact. We’ve shown that drones can be a valuable tool for investigating multi-scalar phenomena, such as how local forest structure combines with environmental conditions to shape forest insect disturbance. Understanding the conditions that drive dry western U.S. forest responses to disturbances such as insect attack will be vital for predicting outcomes of increasing disturbance frequency and intensity. Our study suggests that outcomes will depend on interactions between local forest structure and broad-scale environmental gradients, with the potential for cross-scale interactions to challenge our current understanding of forest insect dynamics.

## Acknowledgements

We gratefully acknowledge funding from the USDA Forest Service Western Wildlands Environmental Threat Assessment Center (WWETAC) and the Pacific Southwest Research Station Climate Change Competitive Grant Program. We thank Connie Millar for comments and guidance during the development of this project and Victoria Scholl for helpful discussions regarding remotely sensed data product levels.

## References

- Anderegg, W. R. L., J. A. Hicke, R. A. Fisher, C. D. Allen, J. Aukema, B. Bentz, S. Hood, J. W. Lichstein, A. K. Macalady, N. McDowell, Y. Pan, K. Raffa, A. Sala, J. D. Shaw, N. L. Stephenson, C. Tague, and M. Zeppel. 2015. Tree mortality from drought, insects, and their interactions in a changing climate. *New Phytologist* 208:674–683.
- Asner, G. P., P. G. Brodrick, C. B. Anderson, N. Vaughn, D. E. Knapp, and R. E. Martin. 2016. Progressive forest canopy water loss during the 2012–2015 California drought. *Proceedings of the National Academy of Sciences* 113:E249–E255.

- 554 Baldwin, B. G., A. H. Thornhill, W. A. Freyman, D. D. Ackerly, M. M. Kling, N. Morueta-Holme, and B. D.  
555 Mishler. 2017. Species richness and endemism in the native flora of California. American Journal of Botany  
556 104:487–501.
- 557 Bedard, W. D., P. E. Tilden, D. L. Wood, R. M. Silverstein, R. G. Brownlee, and J. O. Rodin. 1969.  
558 Western pine beetle: Field response to its sex pheromone and a synergistic host terpene, myrcene. Science  
559 164:1284–1285.
- 560 Bentz, B. J., J. Régnière, C. J. Fettig, E. M. Hansen, J. L. Hayes, J. A. Hicke, R. G. Kelsey, J. F. Negrón,  
561 and S. J. Seybold. 2010. Climate change and bark beetles of the western United States and Canada: Direct  
562 and indirect effects. BioScience 60:602–613.
- 563 Berryman, A. A. 1982. Population dynamics of bark beetles. Pages 264–314 in Bark Beetles in North  
564 American Conifers: A System for the Study of Evolutionary Biology.
- 565 Brooks, S. P., and A. Gelman. 1998. General methods for monitoring convergence of iterative simulations.  
566 Journal of Computational and Graphical Statistics 7:434.
- 567 Bürkner, P.-C. 2017. **brms**: An *R* package for bayesian multilevel models using *Stan*. Journal of Statistical  
568 Software 80.
- 569 Byers, J. A., and D. L. Wood. 1980. Interspecific inhibition of the response of the bark beetles, *Dendroctonus*  
570 *brevicomis* and *Ips paraconfusus*, to their pheromones in the field. Journal of Chemical Ecology 6:149–164.
- 571 Chesson, P. 2000. Mechanisms of maintenance of species diversity. Annual Review of Ecology and Systematics  
572 31:343–366.
- 573 Chubaty, A. M., B. D. Roitberg, and C. Li. 2009. A dynamic host selection model for mountain pine beetle,  
574 *Dendroctonus ponderosae* Hopkins. Ecological Modelling 220:1241–1250.
- 575 Clevers, J., and A. Gitelson. 2013. Remote estimation of crop and grass chlorophyll and nitrogen content using  
576 red-edge bands on Sentinel-2 and -3. International Journal of Applied Earth Observation and Geoinformation  
577 23:344–351.
- 578 Coops, N. C., M. Johnson, M. A. Wulder, and J. C. White. 2006. Assessment of QuickBird high spatial  
579 resolution imagery to detect red attack damage due to mountain pine beetle infestation. Remote Sensing of  
580 Environment 103:67–80.
- 581 DJI. 2015a. Zenmuse X3 - Creativity Unleashed. <https://www.dji.com/zenmuse-x3/info>.
- 582 DJI. 2015b. DJI - The World Leader in Camera Drones/Quadcopters for Aerial Photography. [https:](https://)

- 583 //www.dji.com/matrice100/info.
- 584 DronesMadeEasy. 2018. Map Pilot for DJI on iOS. [https://itunes.apple.com/us/app/map-pilot-for-dji/  
id1014765000?mt=8](https://itunes.apple.com/us/app/map-pilot-for-dji/id1014765000?mt=8).
- 586 Evenden, M. L., C. M. Whitehouse, and J. Sykes. 2014. Factors influencing flight capacity of the mountain  
587 pine beetle (Coleoptera: Curculionidae: Scolytinae). *Environmental Entomology* 43:187–196.
- 588 Eysn, L., M. Hollaus, E. Lindberg, F. Berger, J.-M. Monnet, M. Dalponte, M. Kobal, M. Pellegrini, E.  
589 Lingua, D. Mongus, and N. Pfeifer. 2015. A benchmark of LiDAR-based single tree detection methods using  
590 heterogeneous forest data from the alpine space. *Forests* 6:1721–1747.
- 591 Farr, T. G., P. A. Rosen, E. Caro, R. Crippen, R. Duren, S. Hensley, M. Kobrick, M. Paller, E. Rodriguez, L.  
592 Roth, D. Seal, S. Shaffer, J. Shimada, J. Umland, M. Werner, M. Oskin, D. Burbank, and D. Alsdorf. 2007.  
593 The shuttle radar topography mission. *Reviews of Geophysics* 45.
- 594 Fettig, C. J. 2012. Chapter 2: Forest health and bark beetles. *in* Managing Sierra Nevada Forests. PSW-  
595 GTR-237. USDA Forest Service.
- 596 Fettig, C. J. 2016. Native bark beetles and wood borers in Mediterranean forests of California. Pages 499–528  
597 *in* Insects and diseases of Mediterranean Forest systems. Springer International Publishing, Switzerland.
- 598 Fettig, C. J., and J. Hilszczański. 2015. Management strategies for bark beetles in conifer forests. Pages  
599 555–584 *in* Bark Beetles. Elsevier.
- 600 Fettig, C. J., K. D. Klepzig, R. F. Billings, A. S. Munson, T. E. Nebeker, J. F. Negrón, and J. T. Nowak. 2007.  
601 The effectiveness of vegetation management practices for prevention and control of bark beetle infestations in  
602 coniferous forests of the western and southern United States. *Forest Ecology and Management* 238:24–53.
- 603 Fettig, C. J., S. R. McKelvey, C. P. Dabney, D. P. W. Huber, C. G. Lait, D. L. Fowler, and J. H. Borden. 2012.  
604 Efficacy of “Verbenone Plus” for protecting ponderosa pine trees and stands from *Dendroctonus brevicomis*  
605 (Coleoptera: Curculionidae) attack in British Columbia and California. *Journal of Economic Entomology*  
606 105:1668–1680.
- 607 Fettig, C. J., S. R. McKelvey, and D. P. W. Huber. 2005. Nonhost angiosperm volatiles and Verbenone disrupt  
608 response of western pine beetle, *Dendroctonus brevicomis* (Coleoptera: Scolytidae), to attractant-baited traps.  
609 *Journal of Economic Entomology* 98:2041–2048.
- 610 Fettig, C. J., L. A. Mortenson, B. M. Bulaon, and P. B. Foulk. 2019. Tree mortality following drought in the  
611 central and southern Sierra Nevada, California, U.S. *Forest Ecology and Management* 432:164–178.

- 612 Flint, L. E., A. L. Flint, J. H. Thorne, and R. Boynton. 2013. Fine-scale hydrologic modeling for regional land-  
613 scape applications: The California Basin Characterization Model development and performance. Ecological  
614 Processes 2:25.
- 615 Floyd, M. L., M. Clifford, N. S. Cobb, D. Hanna, R. Delph, P. Ford, and D. Turner. 2009. Relationship of  
616 stand characteristics to drought-induced mortality in three Southwestern piñonJuniper woodlands. Ecological  
617 Applications 19:1223–1230.
- 618 Franceschi, V. R., P. Krokene, E. Christiansen, and T. Krekling. 2005. Anatomical and chemical defenses of  
619 conifer bark against bark beetles and other pests. New Phytologist 167:353–376.
- 620 Frey, J., K. Kovach, S. Stemmler, and B. Koch. 2018. UAV photogrammetry of forests as a vulnerable  
621 process. A sensitivity analysis for a structure from motion RGB-image pipeline. Remote Sensing 10:912.
- 622 Fricker, G. A., N. W. Synes, J. M. Serra-Diaz, M. P. North, F. W. Davis, and J. Franklin. 2019. More than  
623 climate? Predictors of tree canopy height vary with scale in complex terrain, Sierra Nevada, CA (USA).  
624 Forest Ecology and Management 434:142–153.
- 625 Gabry, J., D. Simpson, A. Vehtari, M. Betancourt, and A. Gelman. 2019. Visualization in Bayesian workflow.  
626 Journal of the Royal Statistical Society: Series A (Statistics in Society) 182:389–402.
- 627 Gitelson, A., and M. N. Merzlyak. 1994. Spectral reflectance changes associated with autumn senescence of  
628 *Aesculus hippocastanum* L. And *Acer platanoides* L. Leaves. Spectral features and relation to chlorophyll  
629 estimation. Journal of Plant Physiology 143:286–292.
- 630 Graf, M., M. Reid, B. Aukema, and B. Lindgren. 2012. Association of tree diameter with body size and lipid  
631 content of mountain pine beetles. The Canadian Entomologist 144:467–477.
- 632 Gray, P. C., A. B. Fleishman, D. J. Klein, M. W. McKown, V. S. Bézy, K. J. Lohmann, and D. W. Johnston.  
633 2019. A convolutional neural network for detecting sea turtles in drone imagery. Methods in Ecology and  
634 Evolution 10:345–355.
- 635 Griffin, D., and K. J. Anchukaitis. 2014. How unusual is the 2012-2014 California drought? Geophysical  
636 Research Letters 41:9017–9023.
- 637 Hayes, C. J., C. J. Fettig, and L. D. Merrill. 2009. Evaluation of multiple funnel traps and stand characteristics  
638 for estimating western pine beetle-caused tree mortality. Journal of Economic Entomology 102:2170–2182.
- 639 Hijmans, R. J., J. van Etten, M. Sumner, J. Cheng, A. Bevan, R. Bivand, L. Busetto, M. Canty, D. Forrest,  
640 A. Ghosh, D. Golicher, J. Gray, J. A. Greenberg, P. Hiemstra, I. for M. A. Geosciences, C. Karney, M.

- 641 Mattiuzzi, S. Mosher, J. Nowosad, E. Pebesma, O. P. Lamigueiro, E. B. Racine, B. Rowlingson, A. Shortridge,  
642 B. Venables, and R. Wueest. 2019. *Raster*: Geographic data analysis and modeling.
- 643 Hunziker, P. 2017. *Velox*: Fast raster manipulation and extraction.
- 644 Jactel, H., and E. G. Brockerhoff. 2007. Tree diversity reduces herbivory by forest insects. *Ecology Letters*  
645 10:835–848.
- 646 Jakubowski, M. K., W. Li, Q. Guo, and M. Kelly. 2013. Delineating individual trees from LiDAR data: A  
647 comparison of vector- and raster-based segmentation approaches. *Remote Sensing* 5:4163–4186.
- 648 James, M. R., and S. Robson. 2014. Mitigating systematic error in topographic models derived from UAV  
649 and ground-based image networks. *Earth Surface Processes and Landforms* 39:1413–1420.
- 650 Kane, V. R., M. P. North, J. A. Lutz, D. J. Churchill, S. L. Roberts, D. F. Smith, R. J. McGaughey, J. T.  
651 Kane, and M. L. Brooks. 2014. Assessing fire effects on forest spatial structure using a fusion of Landsat and  
652 airborne LiDAR data in Yosemite National Park. *Remote Sensing of Environment* 151:89–101.
- 653 Kolb, T. E., C. J. Fettig, M. P. Ayres, B. J. Bentz, J. A. Hicke, R. Mathiasen, J. E. Stewart, and A. S. Weed.  
654 2016. Observed and anticipated impacts of drought on forest insects and diseases in the United States. *Forest  
655 Ecology and Management* 380:321–334.
- 656 Kuhn, M. 2008. Building predictive models in R using the caret package. *Journal of Statistical Software*  
657 28:1–26.
- 658 Larson, A. J., and D. Churchill. 2012. Tree spatial patterns in fire-frequent forests of western North America,  
659 including mechanisms of pattern formation and implications for designing fuel reduction and restoration  
660 treatments. *Forest Ecology and Management* 267:74–92.
- 661 Li, W., Q. Guo, M. K. Jakubowski, and M. Kelly. 2012. A new method for segmenting individual trees from  
662 the LiDAR point cloud. *Photogrammetric Engineering & Remote Sensing* 78:75–84.
- 663 Logan, J. A., P. White, B. J. Bentz, and J. A. Powell. 1998. Model analysis of spatial patterns in mountain  
664 pine beetle outbreaks. *Theoretical Population Biology* 53:236–255.
- 665 Meyer, F., and S. Beucher. 1990. Morphological segmentation. *Journal of Visual Communication and Image  
666 Representation* 1:21–46.
- 667 Micasense. 2015. MicaSense. <https://support.micasense.com/hc/en-us/articles/215261448-RedEdge-User-Manual-PDF-Download>
- 668 Millar, C. I., N. L. Stephenson, and S. L. Stephens. 2007. Climate change and forests of the future: Managing  
669 in the face of uncertainty. *Ecological Applications* 17:2145–2151.

- 670 Millar, C. I., R. D. Westfall, D. L. Delany, M. J. Bokach, A. L. Flint, and L. E. Flint. 2012. Forest mortality in  
671 high-elevation whitebark pine (*Pinus albicaulis*) forests of eastern California, USA: Influence of environmental  
672 context, bark beetles, climatic water deficit, and warming. Canadian Journal of Forest Research 42:749–765.
- 673 Miller, J. M., and F. P. Keen. 1960. Biology and control of the western pine beetle: A summary of the first  
674 fifty years of research. US Department of Agriculture.
- 675 Moeck, H. A., D. L. Wood, and K. Q. Lindahl. 1981. Host selection behavior of bark beetles (Coleoptera:  
676 Scolytidae) attacking *Pinus ponderosa*, with special emphasis on the western pine beetle, *Dendroctonus*  
677 *brevicomis*. Journal of Chemical Ecology 7:49–83.
- 678 Morris, J. L., S. Cottrell, C. J. Fettig, W. D. Hansen, R. L. Sherriff, V. A. Carter, J. L. Clear, J. Clement, R.  
679 J. DeRose, J. A. Hicke, P. E. Higuera, K. M. Mattor, A. W. R. Seddon, H. T. Seppä, J. D. Stednick, and S.  
680 J. Seybold. 2017. Managing bark beetle impacts on ecosystems and society: Priority questions to motivate  
681 future research. Journal of Applied Ecology 54:750–760.
- 682 Oliver, W. W. 1995. Is self-thinning in ponderosa pine ruled by *Dendroctonus* bark beetles? Page 6 in Forest  
683 health through silviculture: Proceedings of the 1995 National Silviculture Workshop.
- 684 Pau, G., F. Fuchs, O. Sklyar, M. Boutros, and W. Huber. 2010. EBImage: An R package for image processing  
685 with applications to cellular phenotypes. Bioinformatics 26:979–981.
- 686 Person, H. L. 1928. Tree selection by the western pine beetle. Journal of Forestry 26:564–578.
- 687 Person, H. L. 1931. Theory in explanation of the selection of certain trees by the western pine beetle. Journal  
688 of Forestry 29:696–699.
- 689 Pile, L. S., M. D. Meyer, R. Rojas, O. Roe, and M. T. Smith. 2019. Drought impacts and compounding  
690 mortality on forest trees in the southern Sierra Nevada. Forests 10:237.
- 691 Plowright, A. 2018. ForestTools: Analyzing remotely sensed forest data.
- 692 Raffa, K. F., B. H. Aukema, B. J. Bentz, A. L. Carroll, J. A. Hicke, M. G. Turner, and W. H. Romme. 2008.  
693 Cross-scale drivers of natural disturbances prone to anthropogenic amplification: The dynamics of bark beetle  
694 eruptions. BioScience 58:501–517.
- 695 Raffa, K. F., and A. A. Berryman. 1983. The role of host plant resistance in the colonization behavior and  
696 ecology of bark beetles (Coleoptera: Scolytidae). Ecological Monographs 53:27–49.
- 697 Raffa, K. F., and A. A. Berryman. 1987. Interacting selective pressures in conifer-bark beetle systems: A  
698 basis for reciprocal adaptations? The American Naturalist 129:234–262.

- 699 Raffa, K. F., J.-C. Grégoire, and B. Staffan Lindgren. 2015. Natural history and ecology of bark beetles.  
700 Pages 1–40 *in* Bark Beetles. Elsevier.
- 701 R Core Team. 2018. R: A language and environment for statistical computing. R Foundation for Statistical  
702 Computing, Vienna, Austria.
- 703 Restaino, C., D. Young, B. Estes, S. Gross, A. Wuenschel, M. Meyer, and H. Safford. 2019. Forest  
704 structure and climate mediate drought-induced tree mortality in forests of the Sierra Nevada, USA. Ecological  
705 Applications 0:e01902.
- 706 Rouse, W., R. H. Haas, W. Deering, and J. A. Schell. 1973. Monitoring the vernal advancement and  
707 retrogradation (green wave effect) of natural vegetation. Type II Report, Goddard Space Flight Center,  
708 Greenbelt, MD, USA.
- 709 Roussel, J.-R. 2019. lidRplugins: Extra functions and algorithms for lidR package.
- 710 Roussel, J.-R., D. Auty, F. De Boissieu, and A. S. Meador. 2019. lidR: Airborne LiDAR data manipulation  
711 and visualization for forestry applications.
- 712 Safford, H. D., and J. T. Stevens. 2017. Natural range of variation for yellow pine and mixed-conifer forests  
713 in the Sierra Nevada, Southern Cascades, and Modoc and Inyo National Forests, California, USA. Page 241.
- 714 Seidl, R., J. Müller, T. Hothorn, C. Bässler, M. Heurich, and M. Kautz. 2016. Small beetle, large-scale  
715 drivers: How regional and landscape factors affect outbreaks of the European spruce bark beetle. The Journal  
716 of applied ecology 53:530–540.
- 717 Seybold, S. J., B. J. Bentz, C. J. Fettig, J. E. Lundquist, R. A. Progar, and N. E. Gillette. 2018. Management  
718 of western North American bark beetles with semiochemicals. Annual Review of Entomology 63:407–432.
- 719 Shepherd, W. P., D. P. W. Huber, S. J. Seybold, and C. J. Fettig. 2007. Antennal responses of the western  
720 pine beetle, *Dendroctonus brevicomis* (Coleoptera: Curculionidae), to stem volatiles of its primary host,  
721 *Pinus ponderosa*, and nine sympatric nonhost angiosperms and conifers. Chemoecology 17:209–221.
- 722 Shiklomanov, A. N., B. A. Bradley, K. M. Dahlin, A. M. Fox, C. M. Gough, F. M. Hoffman, E. M. Middleton,  
723 S. P. Serbin, L. Smallman, and W. K. Smith. 2019. Enhancing global change experiments through integration  
724 of remote-sensing techniques. Frontiers in Ecology and the Environment 0.
- 725 Shin, P., T. Sankey, M. Moore, and A. Thode. 2018. Evaluating unmanned aerial vehicle images for estimating  
726 forest canopy fuels in a ponderosa pine stand. Remote Sensing 10:1266.
- 727 Stephenson, N. 1998. Actual evapotranspiration and deficit: Biologically meaningful correlates of vegetation

- 728 distribution across spatial scales. *Journal of Biogeography* 25:855–870.
- 729 Stephenson, N. L., A. J. Das, N. J. Ampersee, and B. M. Bulaon. 2019. Which trees die during drought?
- 730 The key role of insect host-tree selection. *Journal of Ecology*:75.
- 731 Stovall, A. E. L., H. Shugart, and X. Yang. 2019. Tree height explains mortality risk during an intense
- 732 drought. *Nature Communications* 10:1–6.
- 733 Thistle, H. W., H. Peterson, G. Allwine, B. Lamb, T. Strand, E. H. Holsten, and P. J. Shea. 2004. Surrogate
- 734 pheromone plumes in three forest trunk spaces: Composite statistics and case studies. *Forest Science* 50.
- 735 USDAFS. 2019, February 11. Press Release: Survey finds 18 million trees died in California in 2018.
- 736 [https://www.fs.usda.gov/Internet/FSE\\_DOCUMENTS/FSEPRD609321.pdf](https://www.fs.usda.gov/Internet/FSE_DOCUMENTS/FSEPRD609321.pdf).
- 737 Vega, C., A. Hamrouni, S. El Mokhtari, J. Morel, J. Bock, J. P. Renaud, M. Bouvier, and S. Durrieu. 2014.
- 738 PTrees: A point-based approach to forest tree extraction from LiDAR data. *International Journal of Applied*
- 739 *Earth Observation and Geoinformation* 33:98–108.
- 740 Wyngaard, J., L. Barbieri, A. Thomer, J. Adams, D. Sullivan, C. Crosby, C. Parr, J. Klump, S. Raj Shrestha,
- 741 and T. Bell. 2019. Emergent challenges for science sUAS data management: Fairness through community
- 742 engagement and best practices development. *Remote Sensing* 11:1797.
- 743 Young, D. J. N., J. T. Stevens, J. M. Earles, J. Moore, A. Ellis, A. L. Jirka, and A. M. Latimer. 2017.
- 744 Long-term climate and competition explain forest mortality patterns under extreme drought. *Ecology Letters*
- 745 20:78–86.
- 746 Zhang, W., J. Qi, P. Wan, H. Wang, D. Xie, X. Wang, and G. Yan. 2016. An easy-to-use airborne LiDAR
- 747 data filtering method based on cloth simulation. *Remote Sensing* 8:501.